Pretest Comprehensive Analysis for the Urban Air Mobility Side-by-Side Test Stand

Stephen J. Wright
Aerospace Engineer
NASA Ames Research Center
Moffett Field, California, United States

Haley V. Cummings
Mechanical Engineer
NASA Ames Research Center
Moffett Field, California, United States

ABSTRACT

The Urban Air Mobility (UAM) Side-by-Side Test Stand (SBS) is a two-rotor test stand designed and built at NASA Ames Research Center under the Revolutionary Vertical Lift Technology (RVLT) Project. The SBS entered service in the wind tunnel in the latter part of 2021 and allows for the experimental analysis of rotor-rotor interactions for UAM vehicles of the side-by-side variety. The SBS will allow investigation of the effect of numerous variables such as rotor lateral separation, rotor collective pitch, model pitch angle (α), rotor rotation direction, and flight speed. This paper presents performance predictions for the SBS. These predictions, which were generated using CAMRAD II, provided increased assurance of the safe operational limits of the system. Additionally, these results, when compared with future data, will be used for validation of the computational models.

NOTATION

A	area of one rotor disk, ft^2
A_{blade}	blade area of one rotor (thrust-weighted), ft2
A_{proj}	projected area of two rotors, ft^2
b	number of blades
c	blade chord, ft
CDO	mean drag coefficient
C_P	power coefficient, $P/(\rho A {V_{tip}}^3)$
C_T	thrust coefficient, $T/(\rho A {V_{tip}}^2)$
C_T/σ	blade loading coefficient, $T/(\rho A_{blade} {V_{tip}}^2)$
D	rotor diameter, ft
D_e	equivalent drag, lb
FM	figure of merit
H	drag force (shaft axes), lb
L	lift (wind axes), lb
$latcyc$	lateral cyclic, deg
L/D_e	effective lift to drag ratio
$lngcyc$	longitudinal cyclic, deg
M_{tip}	tip Mach number
M_x	roll moment, (x-axis downstream), ft-lb
M_y	pitch moment, (y-axis toward starboard), ft-lb
P	power, lb-ft/s
R	rotor radius, ft
$R1$	rotor 1, starboard rotor
$R2$	rotor 2, port rotor
Re	Reynolds number
RPM	revolutions per minute
$RVLT$	revolutionary vertical lift technology
SBS	Side-by-Side Test Stand
T	thrust (shaft axes), lb
UAM	urban air mobility
V	flight speed, ft/s
V_{tip}	tip speed, ft/s
Y	side force, lb
α	model pitch angle (positive nose up), deg
μ	advance ratio, V/V_{tip}
ρ	air density, slug/ft^3
σ	solidity, A_{blade}/A

INTRODUCTION

In the blossoming Urban Air Mobility (UAM) vehicle design space, there are numerous conceptual designs featuring side-by-side rotors. This configuration is captured in one of the NASA UAM concept vehicles (Fig. 1), which features two, counterrotating, intermeshing rotors (Ref. 1).

Figure 1. NASA's UAM side-by-side concept vehicle

Previously, the side-by-side concept vehicle was studied with comprehensive analysis and computational fluid dynamics (Ref. 2). In that study, cruise performance was computationally shown to benefit with 15% rotor overlap, highlighting the importance of rotor-rotor aerodynamic interactions (Ref. 2). To experimentally study such interactions, the Urban Air Mobility Side-by-Side Test Stand (SBS) was developed as part of the NASA Revolutionary Vertical Lift Technology (RVLT) effort to research potential

Presented at the VFS Aeromechanics for Advanced Vertical Flight Technical Meeting, San Jose, CA, Jan 25-27, 2022.

UAM vehicle technologies. Designed and built at NASA Ames Research Center (Ref. 3), the test stand completed its first test entry in the U.S. Army's 7- by 10-Foot Wind Tunnel in Fall of 2021 and provides NASA and its partners with new testing capabilities for vehicles of side-by-side rotor configurations.

Figure 2 shows the SBS as it was tested in the U.S. Army's 7- by 10-Foot Wind Tunnel. Lateral separation of the two rotors is variable, enabling the experimental investigation of the impact of rotor-to-rotor separation on rotor performance. The two rotor heads are mounted to the strongback, which is mounted to the wind tunnel floor via three struts. The tail strut has an actuator that enables different settings of model pitch angle (α). A single electric motor drives the two rotors through a gearbox assembly. Each rotor is equipped with a swashplate assembly, allowing for collective and cyclic control. The rotors do not have flap or lag hinges, and the blades are untwisted and untapered. Table 1 gives the key parameters of the SBS rotors. Trimming the rotors in the wind tunnel involves modulating thrust with collective and zeroing moments with cyclic control. Each rotor swashplate is controlled independently.

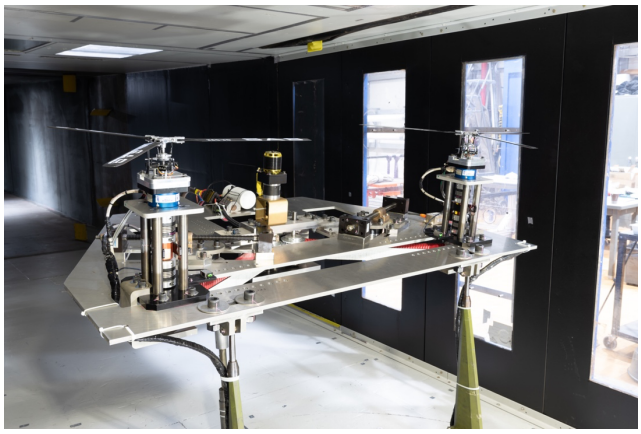

Figure 2. The SBS in the U.S. Army 7- by 10-Foot Wind Tunnel at NASA Ames Research Center

Table 1. Select Model Parameters

Parameter	Value
Number of rotors	2
Number of blades	3
Rotor radius	1.335 ft
Mean chord	0.0976 ft
σ (geometric)	0.07093
Lock number	2.7587
RPM	2500
V_{tip}	349.502 ft/s
M_{tip} (hover)	0.313
Rotor rotation direction	inboard retreating

It was necessary to computationally generate predictions for the expected loads and performance of the system for the pretest documentation and reviews. These predictions are the subject of this paper, and no comparison with experimental data is presented. Such a comparison will be the topic of future work.

APPROACH

Comprehensive Analytical Model of Rotorcraft Aerodynamics and Dynamics (CAMRAD II) (Ref. 4) was used to generate the pretest predictions for loads and performance. Cases were run in both hover and in forward flight with a free wake model and rigid blades. Table 1 tabulates key parameters of the CAMRAD II model used for the analysis.

The CAMRAD II model of the SBS does not include the "airframe" (in this case, the test stand hardware). The primary purpose of this computational model is to investigate rotor performance due to rotor-rotor interactions; thus, neglecting the airframe in the computational model is appropriate.

The results presented in this paper were generated using an NACA 0012 airfoil. Due to the small scale of the rotors, a Reynolds Number (Re) correction was activated within CAMRAD II. This correction scaled drag coefficients in the airfoil tables according to Eqn. 1,

$$(Re_{table}/Re_{model})^{0.125} = 1.48 \qquad \text{(Eqn. 1)}$$

Where $\mathrm{Re}_{\mathrm{table}}$ is the Reynolds number in the airfoil tables, and $\mathrm{Re}_{\mathrm{model}}$ is the Reynolds number of the model, as calculated by CAMRAD II.

Variables of SBS testing include rotor collective pitch, model pitch angle (α), rotor lateral separation, direction of rotor rotation, and tunnel speed. For the CAMRAD II analysis, each of these variables (with the exception of rotation direction) was investigated through various simulations. All CAMRAD II analysis was done with inboard blades retreating for both rotors.

Hover analysis was performed here as a test of the computational model functionality and to predict hovering rotor performance; however, due to inconsistent ground effect caused by the strongback hardware, the SBS is not well-suited to measuring hover performance. The hovering condition is only used for model checkout.

Hover cases were broken down into two different types of studies. Each has its own dedicated section in this paper. The first hover study consisted of untrimmed collective sweeps. Trim was turned off in CAMRAD II, and collective was swept through a wide range of values. The second type of hover study was a series of untrimmed cyclic pitch excursions. These were performed in order to determine the sensitivity of the system to various amounts of lateral and longitudinal cyclic input. Primary interest was given to the impact of hovering-rotor cyclic pitch on the roll and pitch hub moments (M_x and M_y, respectively) of the two rotors.

For forward flight, three different studies were conducted (each has its own designated section in this paper). First, cases were run with trim turned off, hence zero cyclic control. These cases were executed in CAMRAD II as tunnel speed sweeps, with rotor speed, model pitch angle (α), collective, and rotor lateral separation specified for each sweep. The purpose of this study was to understand the potential loads that might be developed if the SBS lost trimming ability (rotor control system failure) in forward flight. The results of these simulations were used in the SBS load and stress analysis.

The second forward flight study was with hub moments trimmed to zero (but thrust untrimmed). Collective sweeps were simulated, with α, tunnel speed, rotor speed, and rotor lateral separation fixed. Cyclic was adjusted to eliminate hub moments. Articulated rotor convention is used for the cyclic, hence "lngcyc" is sine-variation of blade pitch and "latcyc" is cosine-variation of blade pitch, producing respectively roll and pitch moments on the hub for these hingeless rotors. Based on sign convention (positive x-axis downstream, positive y-axis toward starboard, and positive moments following the right-hand rule convention), lngcyc produces a positive roll moment on R1 and negative roll moment on R2. Latcyc produces negative pitch moment on both rotors. The purposes of this study were to determine the blade collective pitch necessary to yield desired levels of thrust and to analyze the performance at different collective settings.

The final type of forward flight study was with moments and thrust trimmed. These cases were simulated as C_T sweeps, with hub moments trimmed to zero and C_T swept through a range of target values. The goal of this study was to simulate the primary method of experimentation performed in the first SBS wind tunnel entry and to determine the performance at different thrust levels.

It was observed that, for certain forward flight cases (particularly certain low thrust cases), there was significant negative loading on the blade, extending inboard of 97% span for some operating conditions. For forward flight, the CAMRAD II wake model accounted for this negative tip loading in the strength of the rolled up tip vortices (the "dual-peak" wake model).

HOVER, UNTRIMMED COLLECTIVE SWEEPS

Hover analysis was performed as a test of the computational model functionality. Table 2 summarizes the cases investigated for the hover, untrimmed collective sweep study. Note that in this paper, a triplet of the form a:b:c refers to a sweep from "a" to "b" with increment "c".

Table 2. Hover, Untrimmed Collective Sweep Cases

Rotor lateral separation (x*D)	Rotor Collective (deg)
1.095	1:22:1
0.907	1:22:1
0.720	1:22:1

Figure 3 is a plot of Figure of Merit (FM) vs C_T/σ for each of the three different settings of rotor lateral separation. Here, FM is calculated according to Eqn. 2,

$$FM = \frac{T_{total}}{P_{total}}\sqrt{\frac{T_{total}}{2\rho A_{proj}}} \qquad \text{(Eqn. 2)}$$

where T_{total} is total thrust (sum of both rotors), P_{total} is total power (sum of both rotors), and A_{proj} is the projected area of the two-rotor system (varies depending on overlap). Figure 3 shows that FM can be increased by reducing the separation (increasing the overlap) of the two rotors. This is mainly due to increased disk loading (which increases ideal power); the increased disk loading is the result of the smaller projected area of the overlapping rotors.

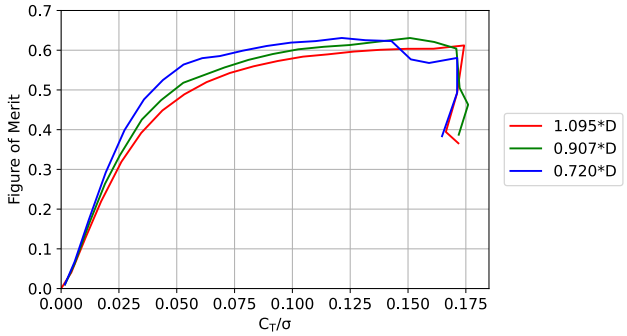

Figure 3. Figure of merit vs C_T/σ for different rotor separations, results averaged between the two rotors

Figure 4 is a plot of C_P/σ vs C_T/σ. This plot highlights the performance characteristics sans the influence of the varying projected area of the two-rotor system.

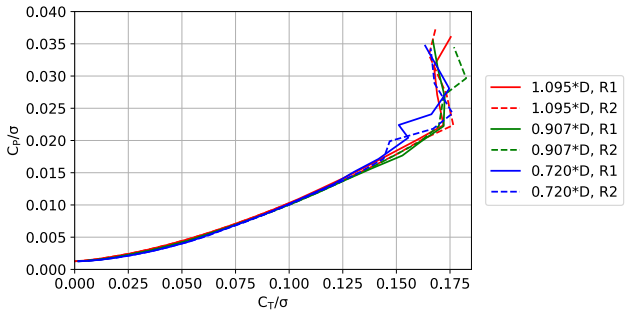

Figure 4. C_P/σ vs C_T/σ for three rotor separations, results shown for both rotors

Figure 5 is a plot of thrust coefficient (C_T/σ) vs collective. From Fig. 4, it can be determined that the rotor achieves the target C_T of 0.01 (C_T/σ of 0.14) at approximately 16.5 deg of blade collective pitch. As collective is increased, the differences between different separations are exacerbated, with 0.720*D lateral separation between rotors underperforming 0.907*D and 1.095*D. The aerodynamics of the wake coupled with blade stall can be chaotic, leading to differences between power and thrust of the two rotors at high thrust.

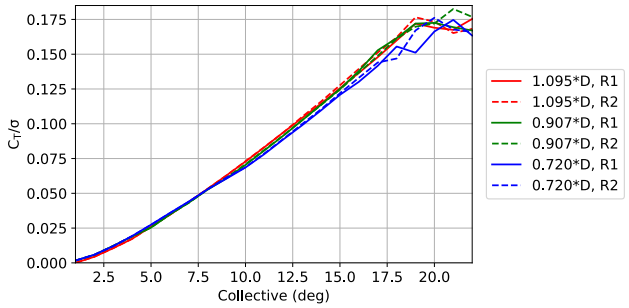

Figure 5. C_T/σ vs collective for different rotor separations, results shown for both rotors

Figures 6 and 7 are plots of M_x and M_y vs collective, respectively. The positive x-axis is downstream, and the positive y-axis is toward starboard. Sign convention for moments follows the right-hand rule convention. Figure 6 shows that the magnitude of M_x increases with increasing collective. Additionally, Fig. 6 shows that the magnitude of M_x is significantly greater with increased rotor overlap. There is no cyclic, so hub moments are caused by rotor-rotor interference. Figure 7 shows that the magnitude of M_y increases with collective, and that the amount of lateral separation between the two rotors causes differences in the amount of M_y.

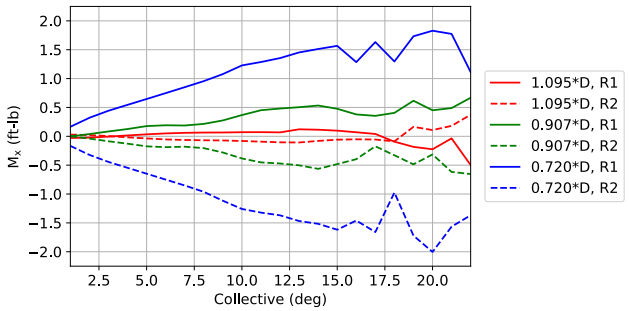

Figure 6. M_x vs collective for three rotor separations, results shown for both rotors

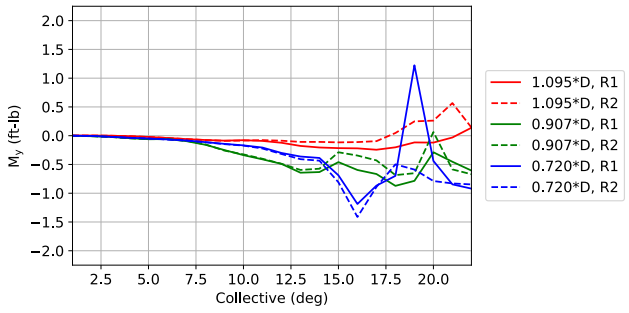

Figure 7. M_y vs collective for three rotor separations, results shown for both rotors

Figure 8 is a plot of side force (Y) vs collective. As can be seen, lateral separation between rotors has a significant impact on the magnitude of Y, with higher levels of overlap yielding greater Y.

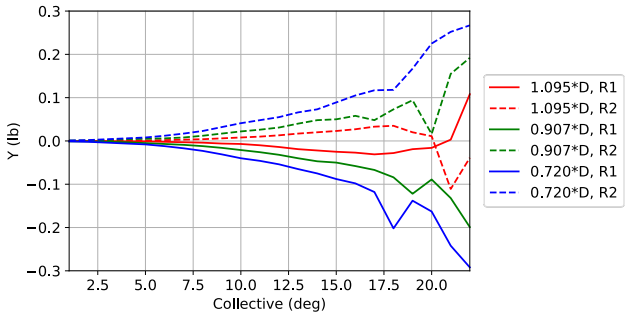

Figure 8. Side force (Y) vs collective for all rotor separations, results shown for both rotors

Figure 9 shows drag force (H) vs collective. Like Y, H force shows significant dependence upon the amount of lateral separation between the two rotors. Up to a collective of about 17.5 deg (which yields C_T beyond the target value of 0.01), higher levels of overlap correspond to greater magnitude H. The disjointed nature of the plot beyond this point is likely due to issues with the numerical solution caused by rotor stall.

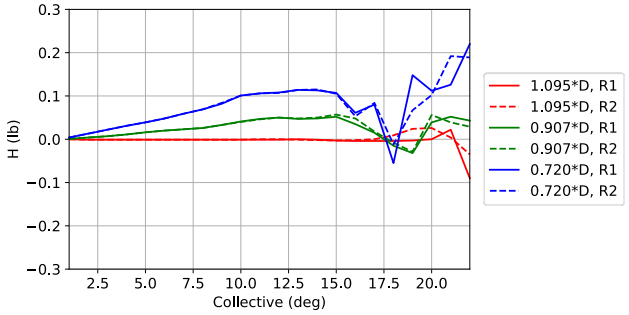

Figure 9. Drag force (H) vs collective for all rotor separations, results shown for both rotors

As mentioned previously, hover analysis was performed here as a test of the computational model functionality; the SBS is not well-suited to measuring hover performance. Any comparison of computational and experimental results will be difficult, if possible at all, due to the ground effect phenomena induced by the SBS hardware.

HOVER, UNTRIMMED CYCLIC STUDY

The hover, untrimmed cyclic study was performed to determine the sensitivity of the system response to cyclic input. Table 3 displays constants for this cyclic study.

Table 3. Constants for Hover, Untrimmed Cyclic Study

Parameter	Value
Collective	16 deg
Rotor-Rotor Separation	0.720*D
Tunnel Speed	0 kts
Rotor Speed	2500 RPM
α	0 deg

Collective of 16 deg was chosen as it yields a C_T value of approximately 0.01 (the target C_T) at 2500 RPM. Various combinations of lateral cyclic (latcyc) and longitudinal cyclic

(lngcyc) were simulated and are summarized in Table 4. For these cases, latcyc and lngcyc were never combined in the same case. Table 4 also presents M_x and M_y for each case. The loads presented here are hub loads, and thus do not include moment caused by the tilting of the thrust vector. The maximum moment in Table 4 is 5.50 lb-ft. This is a roll moment on R1 corresponding to the case with 5 deg of lngcyc applied to R1.

Table 4. Hub Moment Response to Cyclic Input

	Cyclic Input (deg)		Hub Moment (ft-lb)	
Rotor	Latcyc	Lngcyc	M_x	M_y
R1	0	0	1.29	-1.19
R2	0	0	-1.46	-1.41
R1	5	0	1.23	-4.16
R2	0	0	-1.37	-0.95
R1	0	0	1.78	-0.64
R2	5	0	-1.55	-4.20
R1	5	0	1.33	-4.18
R2	5	0	-1.38	-4.14
R1	0	5	5.50	-0.82
R2	0	0	-1.39	-0.79
R1	0	0	1.48	-0.70
R2	0	5	-5.49	-0.75
R1	0	5	5.13	-0.96
R2	0	5	-5.10	-0.98

In addition to the cases presented in Table 4, two sweeps were simulated – one of lateral cyclic and one of longitudinal cyclic. In each of these two sweeps, the same cyclic input was sent to each rotor. The results of these sweeps are presented in Figs. 10-11. Figure 10 indicates that roll moment is relatively unaffected by latcyc input. Note that the difference in sign for M_x of R1 and R2 is due to the different rotational directions of the two rotors. Figure 10 also shows that latcyc input has the effect of generating a pitch moment on the rotors. Conversely, Fig. 11 shows that lngcyc input has the effect of increasing roll moment; pitch moment is relatively unaffected by lngcyc.

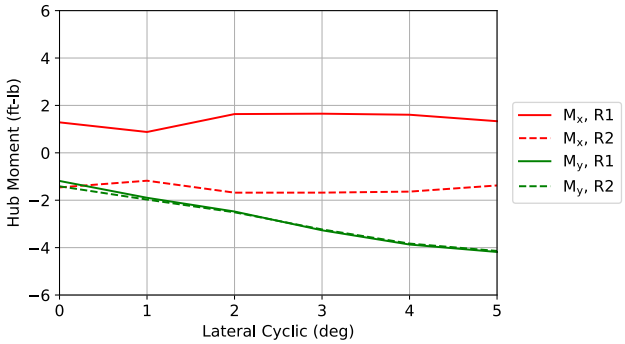

Figure 10. Hover M_x and M_y vs lateral cyclic for 0.720*D rotor separation, results shown for both rotors

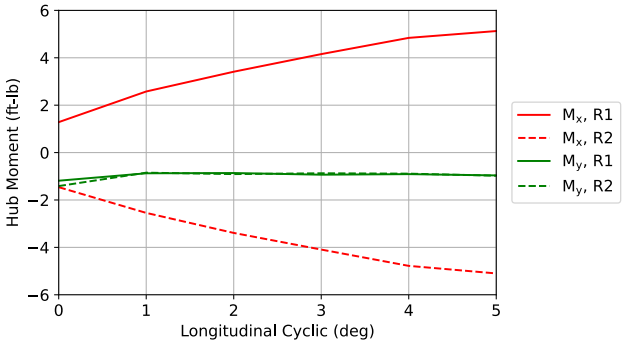

Figure 11. Hover M_x and M_y vs longitudinal cyclic for 0.720*D rotor separation, results shown for both rotors

FORWARD FLIGHT, UNTRIMMED SPEED SWEEPS

The purpose of the forward flight, untrimmed speed sweep study was to understand the potential loads that might be developed if the rotor system lost the ability to trim during forward flight operation. All combinations of the parameters in Table 5 were analyzed.

Table 5. Forward Flight Parameters

Variable	Value
Rotor separation	0.720, 0.907, 1.095 (*D)
Rotor speed	2500 RPM
Tunnel speed	20:60:10 (kts)
Advance ratio (μ)	~ 0.10:0.29:0.05
α	0, -3, -6 (deg)
Collective	4, 8, 12, and 16 (deg)

Additional cases at higher tunnel speeds were analyzed; however, convergence issues occurred around 70 kts. Thus, in this paper, only results up to 60 kts are presented. Some nonconvergent cases are included in this paper if the data fits with that of the convergent cases.

The primary interest was maximum hub moments (M_x and M_y). While the SBS is intended for trimmed operation, it is important to understand the loads that might be encountered if trim cannot be achieved. For each combination of collective and α, a tunnel speed sweep was simulated. From the results of each tunnel speed sweep, the maximums of thrust, M_x, and M_y were extracted and are tabulated in Tables 6, 7, and 8, respectively. The corresponding tunnel speeds and rotor lateral separations are included. For brevity, only R1 results are tabulated.

Table 6 reveals several trends. Thrust increased with collective. Thrust was generally highest at high tunnel speed, as expected for a rotor with fixed collective and cyclic pitch settings. Additionally, increased nose-down α yielded lower thrust, all other parameters being equal. In all but one instance, 0.907*D rotor separation yielded the maximum thrust. This last observation suggests a strong dependence of thrust upon rotor-rotor interactions.

Table 6. Maximum Thrust, R1

α (deg)	Collective (deg)	Max Thrust (lb)	Speed (kts)	Rotor Separation (*D)
0	4	6.7	60	0.907
0	8	13.4	60	0.907
0	12	20.1	60	0.907
0	16	25.1	60	0.720
-3	4	4.7	40	0.907
-3	8	11.3	60	0.907
-3	12	18.0	60	0.907
-3	16	24.0	60	0.907
-6	4	3.9	20	0.907
-6	8	9.4	40	0.907
-6	12	15.9	60	0.907
-6	16	22.5	60	0.907

Table 7 highlights several trends for M_x. In general, M_x is greater at high tunnel speeds, greater at higher collectives, and greater with less nose-down α. In all but one case, M_x was greatest for rotor separation of 0.720*D. This consistent observation suggests that M_x, like thrust, depends significantly upon rotor-rotor interactions.

Table 7. Maximum hub roll moment, R1

α (deg)	Collective (deg)	Max M_x (lb-ft)	Speed (kts)	Rotor Separation (*D)
0	4	2.20	60	0.720
0	8	4.42	60	0.720
0	12	6.69	60	0.720
0	16	8.14	60	0.720
-3	4	1.84	60	0.720
-3	8	4.04	60	0.720
-3	12	6.30	60	0.720
-3	16	8.20	60	0.720
-6	4	1.43	60	0.907
-6	8	3.65	60	0.720
-6	12	5.92	60	0.720
-6	16	8.16	60	0.720

From Table 8, it can be observed that M_y is generally greater with less nose-down α (although this trend is inverted for the highest setting of collective). M_y is also generally greater at lower speeds. Comparing M_x from Table 7 and M_y from Table 8, it is clear that M_x is generally of greater magnitude for these forward flight, untrimmed cases. Interestingly, there is not an obvious trend of maximum M_y with rotor lateral separation, suggesting that M_y is less influenced by rotor-rotor interactions than are thrust and M_x.

Table 8. Maximum hub pitch moment, R1

α (deg)	Collective (deg)	Max M_y (ft-lb)	Speed (kts)	Rotor Separation (*D)
0	4	1.06	20	1.095
0	8	1.71	20	0.907
0	12	2.26	20	0.907
0	16	1.26	20	1.095
-3	4	0.87	20	0.720
-3	8	1.54	20	0.907
-3	12	1.99	20	0.907
-3	16	1.41	40	1.095
-6	4	0.70	20	0.720
-6	8	1.38	20	0.907
-6	12	2.02	20	0.907
-6	16	1.65	30	1.095

FORWARD FLIGHT, MOMENT-TRIMMED COLLECTIVE SWEEPS

The purposes of this study were to determine the blade collective pitch necessary to yield desired levels of thrust and to analyze the performance at different collective settings. Table 9 lists the parameters for these collective sweeps. All combinations of the parameters were simulated and analyzed.

Table 9. Forward Flight Collective Sweep Parameters

Variable	Value
Rotor separation	0.720, 0.907, 1.095 (*D)
Tunnel Speed	20, 40, 60 (kts)
Rotor Speed	2500 RPM
Advance ratio (μ)	0.10, 0.19, 0.29
α	0, -3, -6 (deg)
Collective	1:22:1 (deg)

The results are broken down by forward flight speed, with one subsection for each speed. Within each of these subsections, plots are presented for each of the three settings of α, with each plot having results for the three different settings of rotor lateral separation. Results in the plots are averaged results of the two rotors. Note that the plots are cropped based upon the convergence of the cases in CAMRAD II. For all cases, the higher collective values did not converge.

Speed = 20 kts

Figure 12 shows C_T/σ vs collective at 20 kts with α = 0 deg for different settings of rotor lateral separation. C_T/σ increases linearly with collective until about 14 deg collective, beyond which no significant increases to C_T/σ are observed. The results for each of the different rotor separations are quite similar, with 0.907*D yielding slightly higher C_T/σ than the other two settings of rotor separation. Figure 13 is a plot of mean drag coefficient (CDO) vs collective and reveals the C_T/σ behavior beyond 14 deg collective to be related to rotor stall. CDO is defined by equation 3, where $F(\mu)$ accounts for the increase in mean dynamic pressure of blade section with speed, and C_{P_o} is the rotor profile power coefficient (Ref. 5).

$$CDO = \frac{8C_{Po}/\sigma}{F(\mu)} \qquad \text{(Eq. 3)}$$

A doubling of CDO is an approximate indicator of significant stall on the rotor disk, and thus it can be inferred that by about 14 deg collective, the rotor is stalled. Below about 14 deg collective, CDO is relatively constant. Starting at about 12 deg collective, CDO begins to increase with collective in a nearly exponential manner due to stall on the rotor disk.

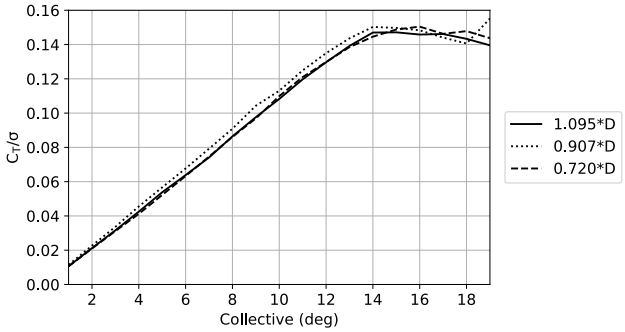

Figure 12. C_T/σ vs collective at 20 kts with α = 0 deg, results for three values of rotor separation

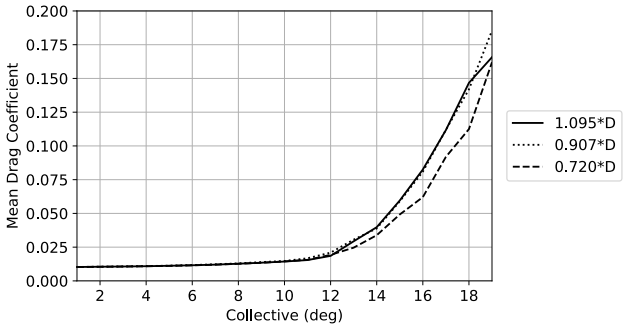

Figure 13. CDO vs collective at 20 kts with α = 0 deg results for three values of rotor separation

Setting α to -3 deg (Fig. 14) and -6 deg (Fig. 15) reveals similar phenomena to the α = 0 deg cases. C_T/σ increases until approximately 14 deg collective, with the 0.907*D rotor separation yielding slightly higher C_T/σ than either of the other two settings of rotor separation. For brevity, CDO plots for these two configurations are not presented; however, it is assumed that stall behavior similar to that of the α = 0 deg cases is the cause of the shift in C_T/σ behavior at approximately 14 deg collective.

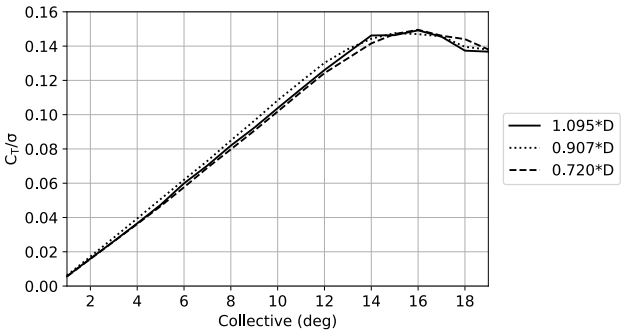

Figure 14. C_T/σ vs collective at 20 kts with α = -3 deg, results for three values of rotor separation

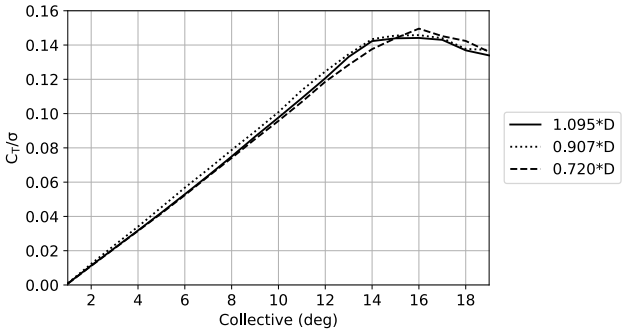

Figure 15. C_T/σ vs collective at 20 kts with α = -6 deg, results for three values of rotor separation

Speed = 40 kts

Figure 16 shows C_T/σ vs collective at 40 kts with α = 0 deg. The leveling out of C_T/σ at about 11 deg of collective is indicative of stall. This is confirmed by Fig. 17, which plots CDO vs collective. CDO doubles by approximately 11 deg collective, indicating stall by this point. The thrust at this speed and model pitch angle is fairly even between the different rotor separations, however 0.907*D still yields slightly higher thrust before stall occurs.

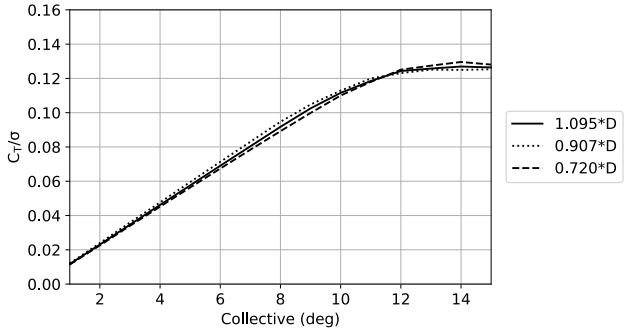

Figure 16. C_T/σ vs collective at 40 kts with α = 0 deg, results for three values of rotor separation

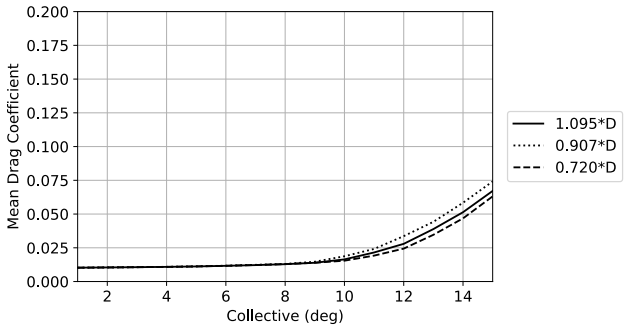

Figure 17. CDO vs collective at 40 kts with α = 0 deg, results for three values of rotor separation

Setting α to -3 deg and -6 deg (Figs. 18 and 19, respectively) reveals similar phenomena to the α = 0 deg cases (Fig. 16). C_T increases linearly until approximately 11-12 deg collective. For brevity, CDO plots for these two configurations are not presented; however, it is assumed that stall is the cause of the shift in C_T behavior at approximately 12 deg collective. It should be noted that with α = -6 deg, C_T is negative at low collective (it is nearly negative with α = -3 deg). This is due to the low collective (low thrust) condition with a significant nose-down rotor orientation.

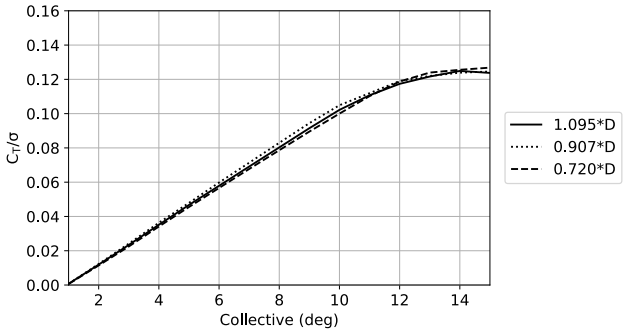

Figure 18. C_T/σ vs collective at 40 kts with α = -3 deg, results for three values of rotor separation

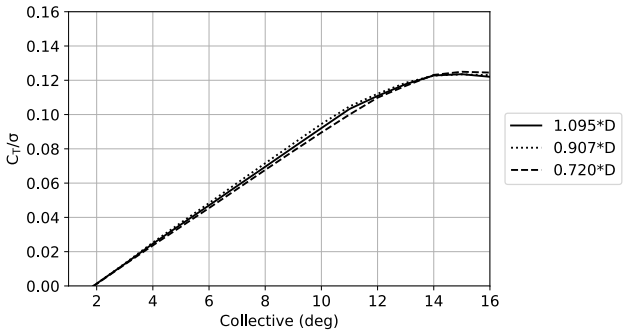

Figure 19. C_T/σ vs collective at 40 kts with α = -6 deg, results for three values of rotor separation

Comparing the results at 40 kts with those at 20 kts, the higher speed cases yield lower C_T/σ values. At 20 kts, max C_T/σ is in excess of 0.14. At 40 kts, maximum C_T/σ is around 0.12. The reduction of maximum rotor lift capability as advance ratio increases is a well-established effect of stall. Additionally, across these cases, the rotor separation distance of 0.907*D yielded slightly higher thrust than either of the other two settings of rotor separation, with this trend being slightly more prominent in the 20 knot cases than in the 40 knot cases.

Speed = 60 kts

Figure 20 shows C_T/σ vs collective at 40 kts with α = 0 deg. The leveling out of C_T/σ at about 11 deg of collective is due to stall. This is confirmed by Fig. 21, which plots CDO vs collective. CDO doubles by approximately 11 deg collective, indicating stall.

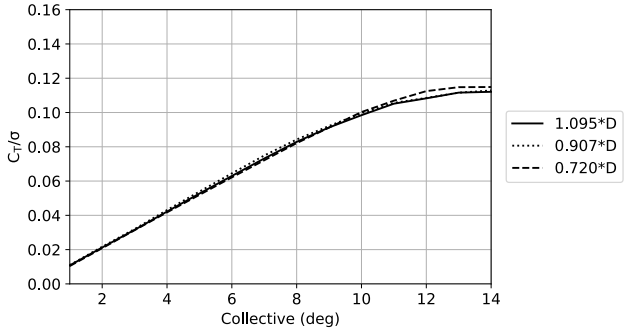

Figure 20. C_T/σ vs collective at 60 kts with α = 0 deg, results for three values of rotor separation

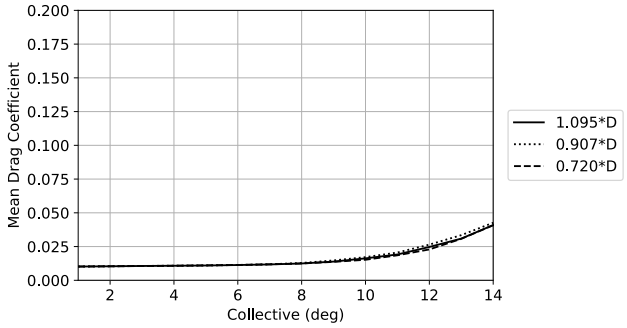

Figure 21. CDO vs collective at 60 kts with α = 0 deg, results for three values of rotor separation

Setting α to -3 deg and -6 deg (Figs. 22 and 23, respectively) reveals similar phenomena to the α = 0 deg cases. C_T/σ increases linearly until approximately 10 deg collective. For brevity, CDO plots for these two configurations are not presented; however, it is assumed that stall is the cause of the shift in C_T/σ behavior at approximately 10 deg collective. It should be noted that with α = -3 and -6 deg, C_T/σ is negative at low collective. As with the 40 kt cases, this negative thrust is likely due to the low collective (low thrust) condition with a significant nose-down rotor orientation.

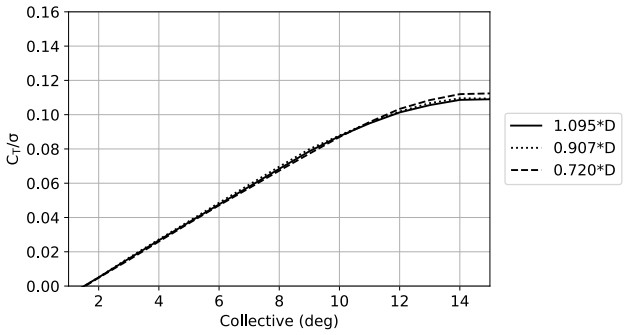

Figure 22. C_T/σ vs collective at 60 kts with α = -3 deg, results for three values of rotor separation

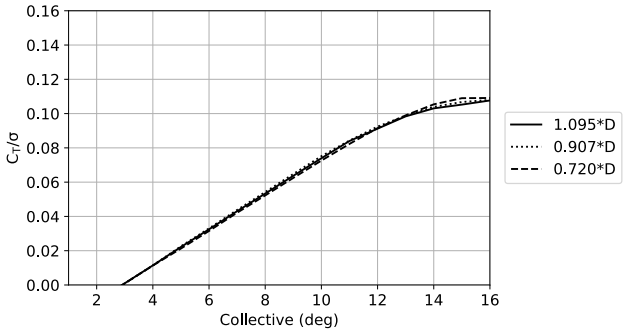

Figure 23. C_T/σ vs collective at 60 kts with α = -6 deg, results for three values of rotor separation

For the 60 kts cases there is not a significant trend observed between the performance of the different rotor lateral separations. Comparing the results at 60 kts with those at 40 kts, it can again be seen that the higher speed cases yield lower C_T/σ values. At 40 kts, maximum C_T/σ is above 0.12. At 60 kts, maximum C_T/σ is between 0.11 and 0.12.

FORWARD FLIGHT, MOMENT-AND-THRUST-TRIMMED C_T SWEEPS

The moment-and-thrust-trimmed C_T sweeps simulated the primary method of experimentation performed in the first SBS wind tunnel entry, yielding performance predictions at different thrust levels. Table 10 tabulates the parameters for these sweeps; all combinations were simulated. Note that in CAMRAD II, the trim quantity was actually C_T/σ, thus the C_T values in Table 10 are approximated. Trimming of C_T/σ was accomplished by modulating collective; RPM was maintained at 2500.

Table 10. Forward Flight C_T Sweep Parameters

Variable	Value
Rotor separation	0.720, 0.907, 1.095 (*D)
Tunnel Speed	20, 40, 60 (kts)
Rotor Speed	2500 RPM
α	0, -3, -6 (deg)
C_T	~ 0.002:0.008:0.001

This section is broken down into three subsections – one for each speed setting. Within each of these three subsections, results are plotted for all values of rotor separation and for all values of α. Note that throughout this section, lines of the same color refer to the same rotor separation. Lines of the same type (solid, dotted, dashed) refer to the same α setting. For plots of effective lift to drag ratio (L/De), L/De is calculated via equation 4,

$$L/D_e = L_{total}V/(P_{total} + VX_{total}) \qquad \text{(Eq. 4)}$$

Where L_{total} is total lift (sum of both rotors), P_{total} is total power (sum of both rotors), and X_{total} is total drag (sum of both rotors).

Speed = 20 kts

Figure 24 is a plot of collective vs C_T for 20 kts. Two trends are observable. Required collective increases with increasing nose-down model pitch angle. Overall, 0.720*D requires the highest collective, followed by 1.095*D. The rotor separation of 0.907*D requires the least collective for the same thrust value.

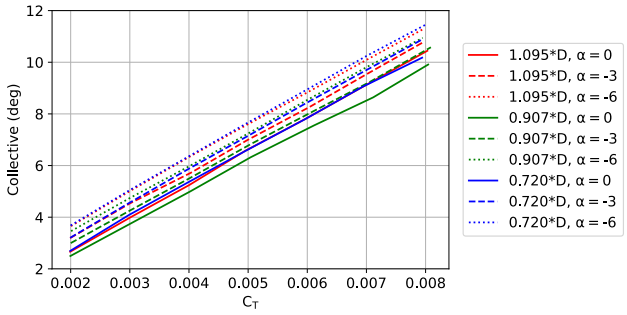

Figure 24. Collective vs C_T at 20 kts, results for three values of rotor separation and three values of α

Figure 25 is a plot of L/D_e vs C_T for 20 kts. Multiple trends are observable. Rotor separation of 0.907*D has the best L/D_e for all values of α. L/D_e generally increases until a C_T value of approximately 0.004. Additionally, L/D_e generally decreases with increasing nose-down model pitch angle.

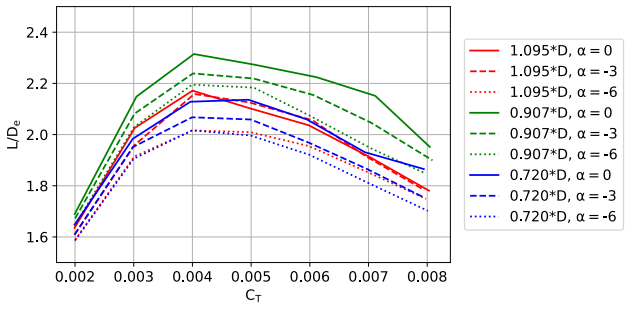

Figure 25. L/D_e vs C_T at 20 kts, results for three values of rotor separation and three values of α

Speed = 40 kts

Figure 26 is a plot of collective vs C_T for 40 kts. Two trends are observable. As before, required collective increases with increasing nose-down model pitch angle. Overall, 0.720*D requires the highest collective, followed by 1.095*D, and

0.907*D requires the least collective to reach the same thrust value.

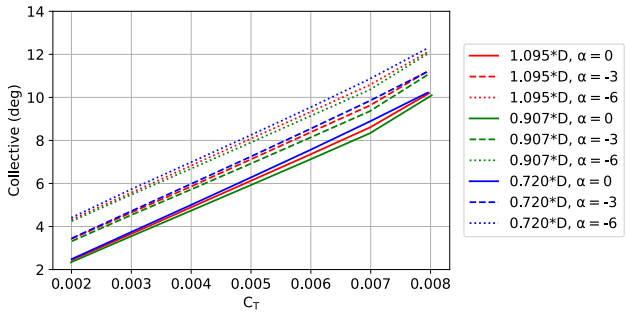

Figure 26. Collective vs C_T at 40 kts, results for three values of rotor separation and three values of α

Figure 27 is a plot of L/D_e vs C_T for 40 kts. Multiple trends are observable. Again, 0.907*D has the best L/D_e. L/D_e generally increases until a C_T of about 0.005. L/D_e decreases with increasing nose-down model pitch angle.

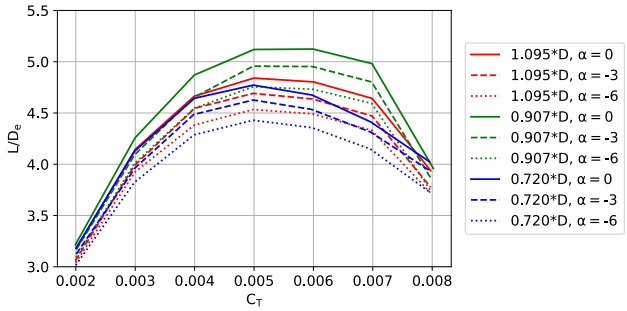

Figure 27. L/D_e vs C_T at 40 kts, results for three values of rotor separation and three values of α

Overall, L/D_e is significantly higher with 40 kts than with 20 kts. Comparing the 0.907*D, α = 0 deg cases, 20 kts has maximum L/D_e of about 2.3, and 40 kts has maximum L/D_e of over 5.0.

Speed = 60 kts

It should be noted that at 60 kts, there were multiple non-convergent cases with α = -6. In particular, C_T = 0.005 and 0.006 did not converge for any cases at 60 kts with α = -6. The non-convergent points are still presented in the plot, as they generally fit with the trend lines of the converged cases.

Figure 28 is a plot of collective vs C_T for 60 kts. Two trends are observable. Required collective increases with increasing nose-down model pitch angle. Overall, up to C_T of about 0.006, 0.720*D requires the highest collective.

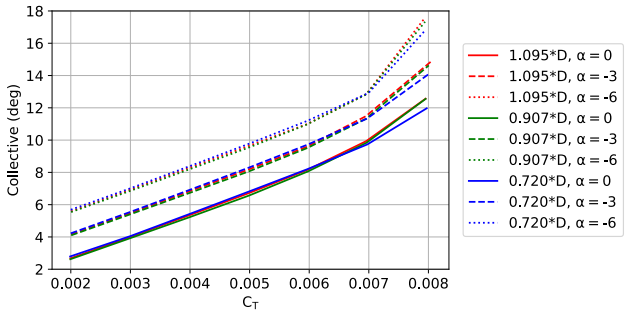

Figure 28. Collective vs C_T at 60 kts, results for three values of rotor separation and three values of α

Figure 29 is a plot of L/D_e vs C_T for 60 kts. Multiple trends are observable. L/D_e generally increases until a C_T of about 0.005. Below this point, 0.907*D has the best L/D_e. Additionally, below 0.005 C_T, L/D_e decreases with increasing nose-down model pitch angle.

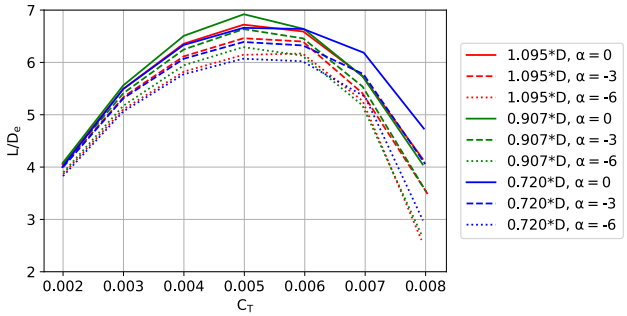

Figure 29. L/D_e vs C_T at 60 kts, results for three values of rotor separation and three values of α

Overall, L/D_e is significantly higher with 60 kts than with 40 kts. Comparing the 0.907*D, α = 0 deg cases, 40 kts has maximum L/D_e of over 5.0, and 60 kts has maximum L/D_e of nearly 7.0.

CONCLUSIONS

Overall conclusions and inferences are presented here, broken down by section.

Untrimmed, hover, collective sweeps

1. Considering Figure of Merit vs C_T/σ (Fig. 3), 0.720*D separation appears to yield the best performance, followed by 0.907*D. However, the increase in FM is largely due to the reduction in projected area caused by increasing rotor overlap.
2. The target C_T value of 0.01 (C_T/σ value of 0.14) requires approximately 16.5 deg rotor collective.
3. M_x decreases with increasing separation (1.095*D yields the smallest M_x).
4. Side force and drag force decrease with increasing separation (1.095*D yields the smallest Y and H).

Untrimmed, hover, cyclic study

1. Lateral and longitudinal cyclic input were shown to have significant impact on resultant hub moments for the untrimmed system in hover. Specifically, lateral cyclic input yielded increased pitching moment. Longitudinal cyclic contributed to an increase in roll moment.

Forward flight, untrimmed speed sweeps

1. Thrust increased with tunnel speed, as expected for rotors with fixed collective and cyclic pitch settings.
2. In all but one instance, 0.907*D rotor separation yielded the maximum thrust.
3. Generally, greater forward α tilt with fixed collective yielded lower thrust.
4. In general, M_x is greater at higher speeds, greater at higher collectives, and greater at lower levels of α. M_x is also generally the greatest for rotor separation of 0.720*D.
5. M_y is generally greater with less α, and it is generally greater at lower speeds.
6. The maximum values of M_x were significantly higher than the maximum values of M_y.
7. There is a strong dependence of thrust and M_x on rotor separation. There is not a clear connection between rotor separation and M_y. This suggests that thrust and M_x both depend significantly upon the rotor-rotor aerodynamic interactions. If M_y also has such a dependence, it seems to be to a lesser degree.

Forward flight, moment-trimmed collective sweeps

1. Highest thrust occurs at the lowest speed (20 kts) and with the highest collective (12 deg or 16 for cases that converged).
2. With α = 0 deg, maximum thrust was about 15.5 lb.
3. With α = -3 deg, maximum thrust was about 15 lb.
4. With α = -6 deg, maximum thrust was about 14.5 lb.

Forward flight, moment-and-thrust-trimmed C_T sweeps

1. L/De generally increases until about C_T =0.004-0.005.
2. Generally, 0.907*D has the best L/D_e.
3. Generally, L/D_e decreases with increasing nose-down model pitch angle
4. L/D_e increases significantly with speed. The 60 kt cases saw far higher max L/D_e than did the 40 kt cases, which in turn had far higher max L/D_e than the 20 kts cases.
5. Required collective increases with increasing nose-down model pitch angle, an expected effect of increasing propulsive force.
6. Overall, 0.720*D requires the highest collective (this breaks down beyond about 0.006 C_T for the 60 kt cases).

Author contact: Stephen Wright stephen.j.wright@nasa.gov
Haley Cummings haley.cummings@nasa.gov

ACKNOWLEDGMENTS

The authors gratefully acknowledge the support of numerous individuals within the NASA Ames Aeromechanics Branch, including Chris Silva and Sarah Conley. Particular, thanks goes to Wayne Johnson. His knowledge of rotorcraft theory and his guidance with the execution of CAMRAD II were invaluable. Thanks also goes to William Warmbrodt for his guidance and mentorship.

REFERENCES

1. Johnson, W., Silva, C., Solis, E., "Concept Vehicles for VTOL Air Taxi Operations," AHS Technical Conference on Aeromechanics Design for Transformative Vertical Flight, San Francisco, CA, January 2018.

2. Diaz, P.V., Johnson, W., Ahmad, J., Yoon, S., "The Side-by-Side Urban Air Taxi Concept," AIAA Aviation Forum 2019, Dallas, TX, 2019.

3. Cummings, H., Willink, G., Silva, C., "Mechanical Design of the Urban Air Mobility Side-by-Side Test Stand," Vertical Flight Society 9th Biennial Autonomous VTOL Technical Meeting, (Virtual), January 2021.

4. Johnson, W., "Rotorcraft Aeromechanics Applications of a Comprehensive Analysis," HeliJapan 1998: AHS International Meeting on Rotorcraft Technology and Disaster Relief, Gifu, Japan, April 1998.

5. Johnson, W., "NDARC. NASA Design and Analysis of Rotorcraft," NASA TP 2015-218751, April 2015.